

TOWARDS ROBUSTNESS AGAINST UNSUSPICIOUS ADVERSARIAL EXAMPLES

Liang Tong¹, Minzhe Guo¹, Atul Prakash², Yevgeniy Vorobeychik¹

¹Washington University in St. Louis, ²University of Michigan
 {liangtong, guominzhe, yvorobeychik}@wustl.edu
 aprakash@umich.edu

ABSTRACT

Despite the remarkable success of deep neural networks, significant concerns have emerged about their robustness to adversarial perturbations to inputs. While most attacks aim to ensure that these are imperceptible, *physical* perturbation attacks typically aim for being unsuspecting, even if perceptible. However, there is no universal notion of what it means for adversarial examples to be unsuspecting. We propose an approach for modeling suspiciousness by leveraging cognitive salience. Specifically, we split an image into foreground (salient region) and background (the rest), and allow significantly larger adversarial perturbations in the background, while ensuring that cognitive salience of background remains low. We describe how to compute the resulting non-salience-preserving dual-perturbation attacks on classifiers. We then experimentally demonstrate that our attacks indeed do not significantly change perceptual salience of the background, but are highly effective against classifiers robust to conventional attacks. Furthermore, we show that adversarial training with dual-perturbation attacks yields classifiers that are more robust to these than state-of-the-art robust learning approaches, and comparable in terms of robustness to conventional attacks.

1 INTRODUCTION

An observation by Szegedy et al. (2014) that state-of-the-art deep neural networks that exhibit exceptional performance in image classification are fragile in the face of small adversarial perturbations of inputs has received a great deal of attention. A series of approaches for designing adversarial examples followed (Szegedy et al., 2014; Goodfellow et al., 2015; Carlini & Wagner, 2017), along with methods for defending against them (Papernot et al., 2016b; Madry et al., 2018), and then new attacks that defeat prior defenses, and so on. Attacks can be roughly classified along three dimensions: 1) introducing small l_p -norm-bounded perturbations, with the goal of these being imperceptible to humans (Madry et al., 2018), 2) using non- l_p -based constraints that capture perceptibility (often called *semantic perturbations*) (Bhattad et al., 2020), and 3) modifying physical objects, such as stop signs (Eykholt et al., 2018), in a way that does not arouse suspicion. One of the most common motivations for the study of adversarial examples is safety and security, such as the potential for attackers to compromise the safety of autonomous vehicles that rely on computer vision (Eykholt et al., 2018). However, while imperceptibility is certainly sufficient for perturbations to be unsuspecting, it is far from necessary, as physical attacks demonstrate. On the other hand, while there are numerous formal definitions that capture whether noise is perceptible (Moosavi-Dezfooli et al., 2016; Carlini & Wagner, 2017), what makes adversarial examples suspicious has been largely informal and subjective.

We propose a simple formalization of an important aspect of what makes adversarial perturbations unsuspecting. Specifically, we make a distinction between image foreground and background, allowing significantly more noise in the background than the foreground. This idea stems from the notion of cognitive salience (Borji et al., 2015; Kümmerer et al., 2017; He & Pugeault, 2018), whereby an image can be partitioned into the two respective regions to reflect how much attention a human viewer pays to the different parts of the captured scene. In effect, we posit that perturbations in the foreground, when visible, will arouse significantly more suspicion (by being cognitively more salient) than perturbations made in the background.

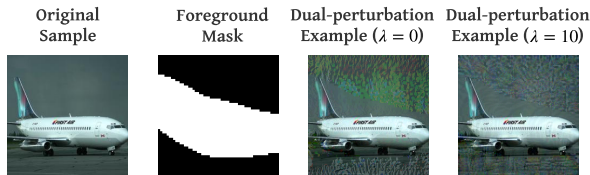


Figure 1: An illustration of dual-perturbation attacks. Adversarial examples are with large ℓ_∞ perturbations on the background ($\epsilon_B = 20/255$) and small ℓ_∞ perturbations on the foreground ($\epsilon_F = 4/255$). A parameter λ is used to control background salience explicitly. A larger λ results in less salient background under the same magnitude of perturbation.

Our first contribution is a formal model of such *dual-perturbation attacks*, which is a generalization of the ℓ_p -norm-bounded attack models (see, e.g., Figure 1), but explicitly aims to ensure that adversarial perturbation does not make the background highly salient. Second, we propose an algorithm for finding adversarial examples using this model, which is an adaptation of the PGD attack (Madry et al., 2018). Third, we present a method for defending against dual-perturbation attacks based on the adversarial training framework (Madry et al., 2018). Finally, we present an extensive experimental study that demonstrates that (a) the proposed attacks are significantly stronger than PGD, successfully defeating all state-of-the-art defenses, (b) proposed defenses using our attack model significantly outperform state-of-the-art alternatives, *with relatively small performance degradation on non-adversarial instances*, and (c) proposed defenses are comparable to, or better than alternatives *even against traditional attacks*, such as PGD.

Related Work: Recent studies have shown that neural networks are vulnerable to adversarial examples. A variety of approaches have been proposed to produce adversarial examples (Szegedy et al., 2014; Goodfellow et al., 2015; Papernot et al., 2016a; Moosavi-Dezfooli et al., 2016; Carlini & Wagner, 2017). These approaches commonly generate adversarial perturbations within a bounded ℓ_p norm so that the perturbations are imperceptible. A related thread has considered the problem of generating adversarial examples that are semantically imperceptible without being small in norm (Brown et al., 2018; Bhattad et al., 2020), for example, through small perturbations to the color scheme. However, none of these account for the perceptual distinction between the foreground and background of images.

Numerous approaches have been proposed for defending neural networks against adversarial examples (Papernot et al., 2016b; Carlini & Wagner, 2017; Madry et al., 2018; Cohen et al., 2019; Madry et al., 2018; Raghunathan et al., 2018). Predominantly, these use ℓ_p -bounded perturbations as the threat model, and while some account for semantic perturbations (e.g. Mohapatra et al. (2020)), none consider perceptually important difference in suspiciousness between foreground and background.

Two recent approaches by Vaishnavi et al. (2019) and Brama & Grinshpoun (2020) have the strongest conceptual connection to our work. Both are defense-focused by either eliminating (Vaishnavi et al., 2019) or blurring (Brama & Grinshpoun, 2020) the background region for robustness. However, they *assume* that we can reliably segment an image *at prediction time*, leaving the approach vulnerable to attacks on image segmentation (Arnab et al., 2018). Xiao et al. (2020) propose to disentangle foreground and background signals on images but unsuspectiousness of their attacks is not ensured.

2 BACKGROUND

2.1 ADVERSARIAL EXAMPLES AND ATTACKS

The problem of generating adversarial examples is commonly modeled as follows. We are given a learned model $h_\theta(\cdot)$ parameterized by θ which maps an input x to a k -dimensional prediction, where k is the number of classes being predicted. The final predicted class y_p is obtained by $y_p = \arg \max_i h_\theta(x)_i$, where $h_\theta(x)_i$ is the i th element of $h_\theta(x)$. Now, consider an input x along with a correct label y . The problem of identifying an adversarial example for x can be captured by



Figure 2: Semantic distinction between foreground and background. Left: Original image of bears. Middle: Adversarial example with ℓ_∞ bounded perturbations ($\epsilon = 40/255$) on the background, the semantic meaning (bear) is preserved. Right: Adversarial example with ℓ_∞ bounded perturbations ($\epsilon = 40/255$) on the foreground, with more ambiguous semantics.

the following optimization problem:

$$\max_{\delta \in \Delta(\epsilon)} \mathcal{L}(h_\theta(\mathbf{x} + \delta), y), \quad (1)$$

where $\mathcal{L}(\cdot)$ is the adversary’s utility function (for example, the loss function used to train the classifier h_θ). $\Delta(\epsilon)$ is the feasible perturbation space which is commonly represented as a ℓ_p ball: $\Delta(\epsilon) = \{\delta : \|\delta\|_p \leq \epsilon\}$.

A number of approaches have been proposed to solve the optimization problem shown in Eq. (1), among which two are viewed as state of the art: *CW attack* developed by Carlini & Wagner (2017), and *Projected Gradient Descent (PGD) attack* proposed in Madry et al. (2018). In this work, we focus on the PGD attack with ℓ_∞ and ℓ_2 as the distance metrics.

2.2 ROBUST LEARNING

An important defense approach that has proved empirically effective even against adaptive attacks is *adversarial training* (Szegedy et al., 2014; Cohen et al., 2019; Goodfellow et al., 2015; Madry et al., 2018). The basic idea of adversarial training is to produce adversarial examples and incorporate these into the training process. Formally, adversarial training aims to solve the following robust learning problem:

$$\min_{\theta} \frac{1}{|D|} \sum_{\mathbf{x}, y \in D} \max_{\|\delta\|_p \leq \epsilon} \mathcal{L}(h_\theta(\mathbf{x} + \delta), y), \quad (2)$$

where D is the training dataset. In practice, this problem is commonly solved by iteratively using the following two steps (Madry et al., 2018): 1) use a PGD (or other) attack to produce adversarial examples of the training data; 2) use any optimizer to minimize the loss of those adversarial examples. It has been shown that adversarial training can significantly boost the adversarial robustness of a classifier against ℓ_p attacks, and it can be scaled to neural networks with complex architectures.

3 DUAL-PERTURBATION ATTACKS

3.1 MOTIVATION

Our threat model is motivated by the *feature integration theory* (Treisman & Gelade, 1980) in cognitive science: regions that have features that are different from their surroundings are more likely to catch a viewer’s gaze. Such regions are called *salient regions*, or *foreground*, while the others are called *background*. Accordingly, for a given image, the semantics of the object of interest is more likely to be preserved in the foreground, as it catches more visual attention of a viewer compared to the background. If the foreground of an image is corrupted, then the semantics of the object of interest is broken. In contrast, the same extent of corruption in the background nevertheless preserves the overall semantic meaning of the scene captured (see, e.g., Figure 2). Indeed, detection of salient regions, as well as the segmentation of foreground and background, have been extensively studied in computer vision (Borji et al., 2015). These approaches either predict human fixations, which are sparse bubble-like salient regions sampled from a distribution (Kümmerer et al., 2017), or salient objects that contain smooth connected areas in an image (He & Pugeault, 2018).

Despite this important cognitive distinction between foreground and background, essentially all of the attacks on deep neural networks for image classification make no such distinction, even though a number of other semantic factors have been considered (Bhattad et al., 2020; Mohapatra et al., 2020). Rather, much of the focus has been on adversarial perturbations that are *not noticeable* to a human, but which are applied equally to the entire image. However, in security applications, the important issue is not merely that an attack cannot be noticed, but that whatever observed is *not suspicious*. This is, indeed, the frame of reference for many high-profile *physical* attacks on image classification, which are clearly visible, but not suspicious because they hide in the “human psyche”, that is, are easily ignored (Sharif et al., 2016; Eykholt et al., 2018). The main goal of the threat model we introduce next is therefore to capture more precisely the notion that an adversarial example is not suspicious by leveraging the cognitive distinction between foreground and background of an image.

3.2 DUAL-PERTURBATION ATTACKS

At the high level, our proposed threat model involves producing small (imperceptible) adversarial perturbations in the foreground of an image, and larger perturbations in the background. This can be done by incorporating state-of-the-art attacks into our method: we can use one attack with small ϵ in the foreground, and another with a large ϵ in the background. Consequently, we term our approach *dual-perturbation attacks*. Note that these clearly generalize the standard small-norm (e.g., PGD) attacks, since we can set the ϵ to be identical in both the foreground and background. However, the key consideration is that after we add the large amount of noise to the background, *we must ensure that we do not thereby make it highly salient to the viewer*. We capture this second objective by including in the optimization problem a *salience* term that decreases with increasing salience of the background.

Formally, the *dual-perturbation* attack solves the following optimization problem:

$$\max_{\|\delta \circ \mathcal{F}(\mathbf{x})\|_p \leq \epsilon_F, \|\delta \circ \mathcal{B}(\mathbf{x})\|_p \leq \epsilon_B} \mathcal{L}(h_{\theta}(\mathbf{x} + \delta), y) + \lambda \cdot \mathcal{S}(\mathbf{x} + \delta), \quad (3)$$

where $\mathcal{S}(\mathbf{x} + \delta)$ measure the relative salience of the foreground compared to background after adversarial noise δ has been added, with λ a parameter that explicitly balances the two objectives: maximizing predicted loss on adversarial examples, and limiting background salience (compared to foreground) so that the adversarial example produced is unsuspecting. Here \mathcal{F} returns the mask matrix constraining the area of the perturbation in the foreground, and \mathcal{B} returns the mask matrix restricting the area of the perturbation in the background, for an input image \mathbf{x} . $\mathcal{F}(\mathbf{x})$ and $\mathcal{B}(\mathbf{x})$ have the same dimension as \mathbf{x} and contain 1s in the area which can be perturbed and 0s elsewhere. \circ denotes element-wise multiplication for matrices. Hence, we have $\mathbf{x} = \mathcal{F}(\mathbf{x}) + \mathcal{B}(\mathbf{x})$ which indicates that any input image can be decomposed into two independent images: one containing just the foreground, and the other containing the background.

We model the suspiciousness $\mathcal{S}(\mathbf{x})$ of an input image \mathbf{x} by leveraging a recent computational model of image salience, DeepGaze II (Kümmerer et al., 2017). DeepGaze II outputs predicted pixel-level density of human fixations on an image with the total density over the entire image summing to 1. Our measure of relative salience of the foreground to background is the *foreground score*, which is defined as $\mathcal{S}(\mathbf{x}) = \sum_{i \in \{k | \mathcal{F}(\mathbf{x})_k \neq 0\}} s_i$, where s_i is the saliency score produced by DeepGaze II for pixel i of image \mathbf{x} . Since foreground, as a fraction of the image, tends to be around 50-60%, a score significantly higher than 0.5 indicates that predicted human fixation is relatively localized to the foreground.

A natural approach for solving the optimization problem shown in Equation 3 is to apply an iterative method, such as the PGD attack. However, the use of this approach poses two challenges in our setting. First, as in the PGD attack, the problem is non-convex, and PGD only converges to a local optimum. We can address this issue by using *random starts*, i.e., by randomly initializing the starting point of the adversarial perturbations, as in Madry et al. (2018). Second, and unlike PGD, the optimization problem in Equation 3 involves *two hard constraints* $\|\delta \circ \mathcal{F}(\mathbf{x})\|_p \leq \epsilon_F$ and $\|\delta \circ \mathcal{B}(\mathbf{x})\|_p \leq \epsilon_B$. Thus, the feasible region of the adversarial perturbation δ is not an ℓ_p ball, which makes computing the projection \mathcal{P}_{ϵ} computationally challenging in high-dimensional settings. To address this challenge, we split the *dual-perturbation* attack into two individual processes in each iteration, one for the adversarial perturbation in the foreground and the other for the background, and then merge these two perturbations when computing the gradients, like a standard PGD attack. Full details of our algorithms for computing dual perturbation examples are provided in Appendix A.

Now, the question that remains is how to partition an input image \mathbf{x} into foreground, $\mathcal{F}(\mathbf{x})$, and background, $\mathcal{B}(\mathbf{x})$. We address this next.

3.3 IDENTIFYING FOREGROUND AND BACKGROUND

Given an input \mathbf{x} , we aim to compute $\mathcal{F}(\mathbf{x})$, the foreground mask and $\mathcal{B}(\mathbf{x})$, the background mask. We consider two approaches for this: fixation prediction and segmentation.

Our first method leverages the fixation prediction approach (Kümmerer et al., 2017) to identify foreground and background. This enables a general approach for foreground-background partition as fixation predictions are not limited to any specific collection of objects. Specifically, we first use DeepGaze II (Kümmerer et al., 2017) to output predicted pixel-level density of human fixations on an image. We then divide the image into foreground and background by setting a threshold $t = 0.5 \cdot (s_{min}(\mathbf{x}) + s_{max}(\mathbf{x}))$ for each input image \mathbf{x} where (s_{min}, s_{max}) are the minimum and maximum values of human fixation on pixels of \mathbf{x} . Pixels with larger values than t are grouped into the foreground, and the others are identified as background subsequently.

Our second approach is to make use of semantic segmentation to provide a partition of the foreground and background in pixel level. This can be done in two steps: First, we use state-of-the-art paradigms for semantic segmentation (e.g., Long et al. (2015)) to identify pixels that belong to each corresponding object, as there might be multiple objects in an image. Next, we identify the pixels that belong to the object of interest as the foreground pixels, and the others as background pixels.

We use both of the above approaches in dual-perturbation attacks when evaluating the robustness of classifiers, as well as designing robust models. More details are available in Section 5.

4 DEFENSE AGAINST DUAL-PERTURBATION ATTACKS

Once we are able to compute the dual-perturbation attack, we can incorporate it into conventional adversarial training paradigms for defense, as it has been demonstrated that adversarial training is highly effective in designing classification models that are robust to a given attack. Specifically, we replace the PGD attack in the adversarial training framework proposed by Madry et al. (2018), with the proposed dual-perturbation attack. We term this approach *AT-Dual*, which aims to solve the following optimization problem:

$$\min_{\theta} \frac{1}{|D|} \sum_{\mathbf{x}, y \in D} \max_{\substack{\|\delta \circ \mathcal{F}(\mathbf{x})\|_p \leq \epsilon_F, \\ \|\delta \circ \mathcal{B}(\mathbf{x})\|_p \leq \epsilon_B}} \mathcal{L}(h_{\theta}(\mathbf{x} + \delta), y) + \lambda \cdot \mathcal{S}(\mathbf{x} + \delta). \quad (4)$$

Note that *AT-Dual* needs to identify background and foreground for any input when solving the inner maximization problems in Equation 4 at training time. At prediction time, our approaches classify test samples like any standard classifiers, which is independent of the semantic partitions so as to close the backdoors to attacks on object detection approaches (Xie et al., 2017). We evaluate the effectiveness of our approaches in Section 5.

5 EXPERIMENTS

5.1 EXPERIMENTAL SETUP

Datasets. We conducted the experiments on the following three datasets (detailed in Appendix B): The first is Segment-6 (Cong & Prakash, 2019), which are images with 32×32 pixels obtained by pre-processing the Microsoft COCO dataset (Lin et al., 2014) to make it compatible with image classification tasks. We directly used the semantic segmentation based foreground masks provided in this dataset. Our second dataset is STL-10, a subset that contains images with 96×96 pixels. Our third dataset is ImageNet-10, a 10-class subset of the ImageNet dataset (Deng et al., 2009). We cropped all its images to be with 224×224 pixels. For STL-10 and ImageNet-10, we used fixation prediction to identify foreground and background as described in Section 3.

Baselines. We consider *PGD* attack as a baseline adversarial model, and *Adversarial Training with PGD Attacks* as a baseline robust classifier. We also consider a classifier trained on non-adversarial

data (henceforth, *Clean*). Additionally, we consider *Randomized Smoothing* (Cohen et al., 2019) and defer the corresponding results to Appendix J.

Evaluation Metrics. We use two standard evaluation metrics for both attacks and defenses: 1) accuracy of prediction on clean test data where no adversarial attacks were attempted. 2) adversarial accuracy, which is accuracy when adversarial inputs are used in place of clean inputs.

Throughout our evaluation, we used both ℓ_2 and ℓ_∞ norms to measure the magnitude of added adversarial perturbations. Due to space limitations, we only present experimental results of the *Clean* model and classification models that are trained to be robust to ℓ_2 norm attacks using the ImageNet-10 dataset. The results for ℓ_∞ norm and other datasets are similar and deferred to Appendix.

In the following experiments, all classifiers were trained with 20 epochs on a ResNet34 model (He et al., 2016) pre-trained on ImageNet and with a customized final fully connected layer. Specifically, we trained AT-PGD by using 50 steps of ℓ_2 PGD attack with $\epsilon = 2.0$, and AT-Dual by using 50 steps of ℓ_2 dual-perturbation attack with $\{\epsilon_F, \epsilon_B, \lambda\} = \{2.0, 20.0, 0.0\}$ at each training epoch. At test time, we used both ℓ_2 PGD and dual-perturbation attacks with 100 steps to evaluate robustness.

5.2 SALIENCY ANALYSIS OF DUAL-PERTURBATION ADVERSARIAL EXAMPLES

We begin by considering a natural question: is our particular distinction between foreground and background actually consistent with cognitive saliency? In fact, this gives rise to two distinct considerations: 1) whether foreground as we identify it is in fact significantly more salient than the background, and 2) if so, whether background becomes significantly more salient *as a result of our dual-perturbation attacks*. We answer both of these questions by appealing to DeepGaze II (Kümmerer et al., 2017) to compute the *foreground score (FS)* of dual-perturbation examples as described in Section 3, and using the accuracy of different classifiers on dual-perturbation examples with different background salience.

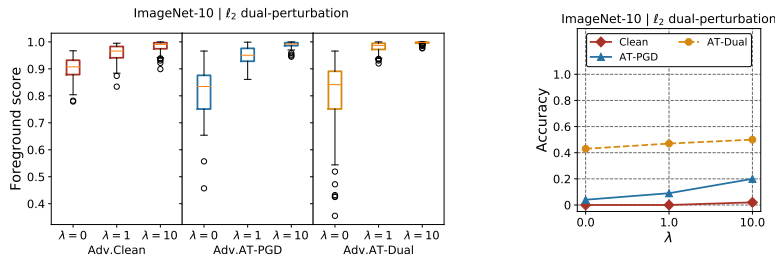


Figure 3: Saliency analysis. Dual-perturbation attacks are performed by using $\{\epsilon_F, \epsilon_B\} = \{2.0, 20.0\}$ and a variety of λ displayed in the figure. Left: foreground scores of dual-perturbation examples in response to different classifiers. Right: accuracy of classifiers on dual-perturbation examples with salience control.

Figure 3 presents the answer to both of the questions above. First, observe that in Figure 3, *FS* (vertical axis) is typically well above 0.5, and in most cases above 0.9, for all attacks. Second, this is true whether we attack the *Clean* model, or either *AT-PGD* or *AT-Dual* robust models. Particularly noteworthy, however, is the impact that the parameter λ has on the *FS*, especially when robust classifiers are employed. Recall that λ reflects the relative importance of salience in generating adversarial examples, with larger values forcing our approach to pay more attention to preserving unsuspectiveness of background relative to foreground. As we increase λ , we note significantly higher *FS*, i.e., lower background salience (again, Figure 3, left). Figure 1 offers a visual illustration of this effect.

As significantly, Figure 3 (right) shows that moderately increasing λ does not significantly reduce the effectiveness of the attack, on either the *Clean* or the robust classifiers.

5.3 DUAL-PERTURBATION ATTACKS ON ROBUST CLASSIFIERS

Next, we evaluate the effectiveness of dual-perturbation attacks against state-of-the-art robust learning methods, as well as the effectiveness of adversarial training that uses dual-perturbation attacks for

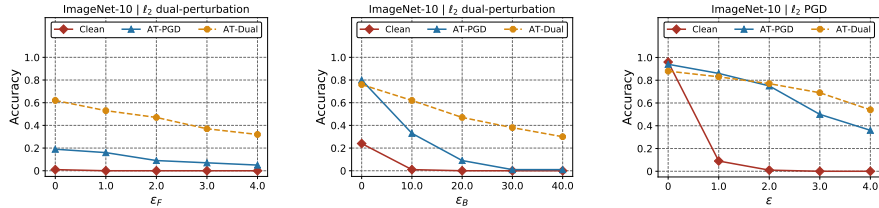


Figure 4: Robustness to white-box ℓ_2 attacks on ImageNet-10. Left: dual-perturbation attacks with different foreground distortions. ϵ_B is fixed to be 20.0 and $\lambda = 1.0$. Middle: dual-perturbation attacks with different background distortions. ϵ_F is fixed to be 2.0 and $\lambda = 1.0$. Right: PGD attacks.

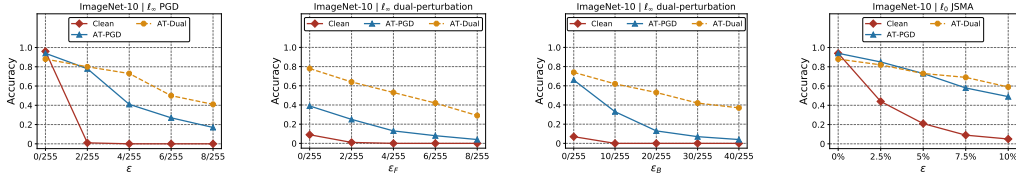


Figure 5: Robustness to additional white-box attacks on ImageNet-10. Left: 20 steps of ℓ_∞ PGD attacks. Middle left: 20 steps of ℓ_∞ dual-perturbation attacks with different foreground distortions. ϵ_B is fixed to be 20/255 and $\lambda = 1.0$. Middle right: 20 steps of ℓ_∞ dual-perturbation attacks with different background distortions. ϵ_F is fixed to be 4/255 and $\lambda = 1.0$. Right: ℓ_0 JSMA attacks.

generating adversarial examples. We begin by considering white-box attacks, and subsequently evaluate transferability. Due to space limitations, we defer the results of transferability to Appendix D.

The results for white-box attacks are presented in Figure 4. First, consider the dual-perturbation attacks (left and middle plots). Note that in all cases these attacks are highly successful against the baseline robust classifier (AT-PGD); indeed, even relatively small levels of foreground noise yield near-zero accuracy when accompanied by sufficiently large background perturbations. For example, when the perturbation to the foreground is $\epsilon_F = 2.0$ and background perturbation is $\epsilon_B = 20.0$, AT-PGD achieves robust accuracy below 10%. In contrast, AT-Dual remains significantly more robust, with an improvement of up to 40% compared to the baseline. Second, consider the standard PGD attacks (right plot). It can be observed that all of the robust models are successful against the ℓ_2 PGD attacks. However, our defense exhibit moderately higher robustness than the baselines under large distortions of PGD attacks, without sacrificing much in accuracy on clean data. For example, when the perturbation of the ℓ_2 PGD attack is above $\epsilon = 3.0$, AT-Dual can achieve 20% more accuracy.

5.4 GENERALIZABILITY OF DEFENSE

It has been observed that models robust against l_p -norm-bounded attacks for one value of p can be fragile when facing attacks with a different norm $l_{p'}$ (Sharma & Chen, 2018). Here, our final goal is to present evidence that the approaches for defense based on dual-perturbation attacks remain relatively robust even when faced with attacks generated using different norms. Here, we show this when our models are trained using the l_2 -bounded attacks, and evaluated against other attacks using other norms. The results are presented in Figure 5. We consider three alternative attacks: 1) PGD using the l_∞ -bounded perturbations, as in Madry et al. (2018) (left in Figure 5) 2) dual-perturbation attacks with l_∞ -norm bounds (middle left and middle right in Figure 5), and 3) JSMA, a l_0 -bounded attack (Papernot et al., 2016a) (right in Figure 5). We additionally considered l_2 attacks, per Carlini and Wagner (Carlini & Wagner, 2017), but find that all of the robust models, whether based on PGD or dual-perturbation attacks, are successful against these.

Our first observation is that AT-Dual is significantly more robust to l_∞ -bounded PGD attacks than the adversarial training approach in which adversarial examples are generated using l_2 -bounded PGD attacks (Figure 5 (left)). Consequently, training with dual-perturbation attacks already exhibits better ability to generalize to other attacks compared to conventional adversarial training.

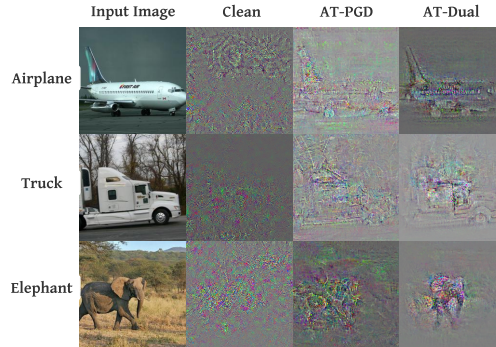


Figure 6: Visualization of loss gradient of different classifiers with respect to pixels of *non-adversarial* inputs.

The gap between dual-perturbation-based adversarial training and standard adversarial training is even more significant when we consider l_∞ dual-perturbation attacks (middle left and middle right figures of Figure 5). Here, we see that robustness of PGD-based adversarially trained model is only marginally better than that of a clean model under large distortions (e.g., when $\epsilon_B \geq 20/255$ in the middle right plot of Figure 5), whereas *AT-Dual* remains relatively robust.

Finally, considering JSMA attacks (see Figure 5 (right)), we can observe that both *AT-Dual* and *AT-PGD* remain relatively robust. However, a deeper look at Figure 5 (right) reveals that compared to *AT-PGD*, *AT-Dual* exhibit moderately higher robustness than the baselines under large distortions of JSMA attacks. Overall, in all of the cases, the model made robust using dual-perturbation attacks remains quite robust even as we evaluate against a different attack, using a different norm.

5.5 ANALYSIS OF DEFENSE

Finally, we conduct an exploratory experiment to study adversarial robustness by investigating which pixel-level features are important for different classifiers at prediction time. To do this, we visualize the loss gradient of different classifiers with respect to pixels of the same *non-adversarial* inputs (as introduced in Tsipras et al. (2019)), shown in Figure 6. Our first observation is that the gradients in response to adversarially robust classifiers (*AT-PGD* and *AT-Dual*) align well with human perception, while a standard training model (*Clean*) results in a noisy gradient for the input images. Second, compared to adversarial training with the conventional PGD attack (*AT-PGD*), the loss gradient of *AT-Dual* provides significantly better alignment with sharper foreground edges and less noisy background. This indicates that adversarial training with the dual-perturbation attack which models unsuspectingness can extract more perceptual semantics from an input image and are less dependant on the background at prediction time. In other words, our defense approach can extract highly robust and semantically meaningful features, which contribute to its robustness to a variety of attacks.

6 CONCLUSION

In this paper, we proposed the dual-perturbation attack, a novel threat model that produces *unsuspecting adversarial examples* by leveraging the cognitive distinction between image foreground and background. As we have shown, our attack can defeat all state-of-the-art defenses. By contrast, the proposed defense approaches using our attack model can significantly improve robustness against unsuspecting adversarial examples, with relatively small performance degradation on non-adversarial data. In addition, our defense approaches can achieve comparable to, or better robustness than the alternatives in the face of traditional attacks.

Our threat model and defense motivate several new research questions. The first is whether there are more effective methods to identify foreground of images. Second, can we further improve robustness to dual-perturbation attacks? Finally, while we provide the first principled approach for quantifying suspiciousness, there may be effective alternative approaches for doing so.

REFERENCES

- Anurag Arnab, Ondrej Miksik, and Philip HS Torr. On the robustness of semantic segmentation models to adversarial attacks. In *IEEE Conference on Computer Vision and Pattern Recognition*, pp. 888–897, 2018.
- Anand Bhattad, Min Jin Chong, Kaizhao Liang, Bo Li, and David Forsyth. Unrestricted adversarial examples via semantic manipulation. In *International Conference on Learning Representations*, 2020.
- Ali Borji, Ming-Ming Cheng, Huaizu Jiang, and Jia Li. Salient object detection: A benchmark. *IEEE transactions on image processing*, 24(12):5706–5722, 2015.
- Haya Brama and Tal Grinshpoun. Heat and blur: An effective and fast defense against adversarial examples. *arXiv preprint*, 2020.
- Tom B. Brown, Nicholas Carlini, Chiyuan Zhang, Catherine Olsson, Paul Christiano, and Ian Goodfellow. Unrestricted adversarial examples. *arXiv preprint*, 2018.
- Nicholas Carlini and David A. Wagner. Towards evaluating the robustness of neural networks. *IEEE Symposium on Security and Privacy*, pp. 39–57, 2017.
- Jeremy M. Cohen, Elan Rosenfeld, and J. Zico Kolter. Certified adversarial robustness via randomized smoothing. In *International Conference on Machine Learning*, 2019.
- Tianji Cong and Atul Prakash. Masked MS-COCO for robust image classification. https://github.com/superctj/Masked_MSCOCO, 2019.
- J. Deng, W. Dong, R. Socher, L. Li, Kai Li, and Li Fei-Fei. Imagenet: A large-scale hierarchical image database. In *2009 IEEE Conference on Computer Vision and Pattern Recognition*, pp. 248–255, 2009.
- Kevin Eykholt, Ivan Evtimov, Earlene Fernandes, Bo Li, Amir Rahmati, Chaowei Xiao, Atul Prakash, Tadayoshi Kohno, and Dawn Xiaodong Song. Robust physical-world attacks on deep learning visual classification. *IEEE/CVF Conference on Computer Vision and Pattern Recognition*, pp. 1625–1634, 2018.
- Ian Goodfellow, Jonathon Shlens, and Christian Szegedy. Explaining and harnessing adversarial examples. In *International Conference on Learning Representations*, 2015.
- Kaiming He, Xiangyu Zhang, Shaoqing Ren, and Jian Sun. Deep residual learning for image recognition. In *Proceedings of the IEEE conference on computer vision and pattern recognition*, pp. 770–778, 2016.
- Sen He and Nicolas Pugeault. Salient region segmentation. *arXiv preprint*, 2018.
- Diederik P Kingma and Jimmy Ba. Adam: A method for stochastic optimization. *arXiv preprint arXiv:1412.6980*, 2014.
- M. Kümmerer, T. S. A. Wallis, L. A. Gatys, and M. Bethge. Understanding low- and high-level contributions to fixation prediction. In *IEEE International Conference on Computer Vision*, 2017.
- Tsung-Yi Lin, Michael Maire, Serge Belongie, James Hays, Pietro Perona, Deva Ramanan, Piotr Dollár, and C Lawrence Zitnick. Microsoft coco: Common objects in context. In *European conference on computer vision*, pp. 740–755. Springer, 2014.
- Jonathan Long, Evan Shelhamer, and Trevor Darrell. Fully convolutional networks for semantic segmentation. In *Proceedings of the IEEE conference on computer vision and pattern recognition*, pp. 3431–3440, 2015.
- Aleksander Madry, Aleksandar Makelov, Ludwig Schmidt, Dimitris Tsipras, and Adrian Vladu. Towards deep learning models resistant to adversarial attacks. In *International Conference on Learning Representations*, 2018.

- Jeet Mohapatra, Tsui Wei Weng, Pin-Yu Chen, Sijia Liu, and Luca Daniel. Towards verifying robustness of neural networks against semantic perturbations. In *International Conference on Learning Representations*, 2020.
- Seyed-Mohsen Moosavi-Dezfooli, Alhussein Fawzi, and Pascal Frossard. Deepfool: a simple and accurate method to fool deep neural networks. In *Proceedings of the IEEE conference on computer vision and pattern recognition*, pp. 2574–2582, 2016.
- Nicolas Papernot, Patrick McDaniel, Somesh Jha, Matt Fredrikson, Z Berkay Celik, and Ananthram Swami. The limitations of deep learning in adversarial settings. In *IEEE European Symposium on Security and Privacy (EuroS&P)*, pp. 372–387, 2016a.
- Nicolas Papernot, Patrick McDaniel, Xi Wu, Somesh Jha, and Ananthram Swami. Distillation as a defense to adversarial perturbations against deep neural networks. In *IEEE Symposium on Security and Privacy (SP)*, pp. 582–597, 2016b.
- Aditi Raghunathan, Jacob Steinhardt, and Percy Liang. Certified defenses against adversarial examples. In *International Conference on Learning Representations*, 2018.
- Mahmood Sharif, Sruti Bhagavatula, Lujo Bauer, and Michael K. Reiter. Accessorize to a crime: Real and stealthy attacks on state-of-the-art face recognition. In *ACM SIGSAC Conference on Computer and Communications Security*, pp. 1528–1540, 2016.
- Yash Sharma and Pin-Yu Chen. Attacking the madry defense model with l_1 -based adversarial examples. In *ICLR-18 Workshops*, 2018.
- Christian Szegedy, Wojciech Zaremba, Ilya Sutskever, Joan Bruna, Dumitru Erhan, Ian Goodfellow, and Rob Fergus. Intriguing properties of neural networks. In *International Conference on Learning Representations*, 2014.
- Anne M Treisman and Garry Gelade. A feature-integration theory of attention. *Cognitive psychology*, 12(1):97–136, 1980.
- Dimitris Tsipras, Shibani Santurkar, Logan Engstrom, Alexander Turner, and Aleksander Madry. Robustness may be at odds with accuracy. In *International Conference on Learning Representations*, 2019.
- Pratik Vaishnavi, Tianji Cong, Kevin Eykholt, Atul Prakash, and Amir Rahmati. Can attention masks improve adversarial robustness? *arXiv preprint*, 2019.
- Kai Xiao, Logan Engstrom, Andrew Ilyas, and Aleksander Madry. Noise or signal: The role of image backgrounds in object recognition. *arXiv preprint*, 2020.
- Cihang Xie, Jianyu Wang, Zhishuai Zhang, Yuyin Zhou, Lingxi Xie, and Alan Yuille. Adversarial examples for semantic segmentation and object detection. In *Proceedings of the IEEE International Conference on Computer Vision*, pp. 1369–1378, 2017.

A DETAILED DESCRIPTIONS OF THE ALGORITHM FOR COMPUTING DUAL-PERTURBATION EXAMPLES

We use the following steps to solve the optimization problem of dual-perturbation attacks:

1. *Initialization.* Start with a random initial starting point $\delta^{(0)}$. To do this, randomly sample a data point $\delta_F^{(0)}$ in ℓ_p ball $\Delta(\epsilon_F)$ and $\delta_B^{(0)}$ in $\Delta(\epsilon_B)$. Then, $\delta^{(0)}$ can be obtained by using $\delta^{(0)} = \delta_F^{(0)} \circ \mathcal{F}(\mathbf{x}) + \delta_B^{(0)} \circ \mathcal{B}(\mathbf{x})$. This ensures that the initial perturbation is feasible in both foreground and background.
2. *Split.* At the k -th iteration, split the perturbation $\delta^{(k)}$ into $\delta_F^{(k)}$ for foreground and $\delta_B^{(k)}$ for background:

$$\begin{cases} \delta_F^{(k)} = \delta^{(k)} \circ \mathcal{F}(\mathbf{x}) \\ \delta_B^{(k)} = \delta^{(k)} \circ \mathcal{B}(\mathbf{x}) \end{cases} . \quad (5)$$

Then update the foreground and background perturbations separately using the following rules:

$$\begin{cases} \delta_F^{(k+1)} = \mathcal{P}_\epsilon(\delta_F^{(k)} + \alpha_F \cdot g_F) \\ \delta_B^{(k+1)} = \mathcal{P}_\epsilon(\delta_B^{(k)} + \alpha_B \cdot g_B) \end{cases} \quad (6)$$

where g_F is the update that corresponds to the *normalized steepest descent* constrained in the foreground, and g_B for the background. Specifically,

$$\begin{cases} g_F = \mathcal{G}(\mathcal{F}(\mathbf{x}) \circ \nabla_{\delta^{(k)}} \{\mathcal{L}(h_\theta(\mathbf{x} + \delta^{(k)}), y)\} + \lambda \cdot \mathcal{S}(\mathbf{x} + \delta^{(k)})) \\ g_B = \mathcal{G}(\mathcal{B}(\mathbf{x}) \circ \nabla_{\delta^{(k)}} \{\mathcal{L}(h_\theta(\mathbf{x} + \delta^{(k)}), y)\} + \lambda \cdot \mathcal{S}(\mathbf{x} + \delta^{(k)})) \end{cases} \quad (7)$$

where α_F is the stepsize for foreground, and α_B is the stepsize for background.

3. *Merge.* At the end of the k -th iteration, merge the perturbations obtained in the last step by using

$$\delta^{(k+1)} = \delta_F^{(k+1)} + \delta_B^{(k+1)}. \quad (8)$$

$\delta^{(k+1)}$ is further used to derive the update for the normalized steepest descent at the next iteration.

4. Return to step 2 or terminate after either a fixed number of iterations.

B DESCRIPTIONS OF DATASETS

B.1 SEGMENT-6

The statistics of the Segment-6 dataset are displayed in Table 1.

Class	Number of samples	
	Training	Test
Train	3,000	200
Bird	3,000	200
Cat	3,000	200
Dog	3,000	200
Toilet	3,000	200
Clock	3,000	200
Total	18,000	1,200

Table 1: Number of samples in each class of the Segment-6 dataset.

B.2 STL-10

The statistics of the STL-10 dataset are displayed in Table 2.

Class	Number of samples	
	Training	Test
Airplane	500	10
Bird	500	10
Car	500	10
Cat	500	10
Deer	500	10
Dog	500	10
Horse	500	10
Monkey	500	10
Ship	500	10
Truck	500	10
Total	5,000	100

Table 2: Number of samples in each class of the STL-10 dataset.

B.3 IMAGENET-10

The labels and number of images per class in the ImageNet-10 dataset are listed in Table 3.

Class	Number of samples	
	Training	Test
Airplane	500	10
Car	500	10
Cat	500	10
Dog	500	10
Truck	500	10
Elephant	500	10
Zebra	500	10
Bus	500	10
Bear	500	10
Bicycle	500	10
Total	5,000	100

Table 3: Number of samples in each class of the ImageNet-10 dataset.

C IMPLEMENTATIONS

We implemented all the attack model, as well as the defense approaches in PyTorch¹, an open-source library for neural network learning. We used the ResNet34 model (He et al., 2016) and standard transfer learning, as the datasets employed in our experiments do not have a sufficient amount of data to achieve high accuracy. Specifically, we initialized the network with the model pre-trained on ImageNet, reset the final fully connected layer, and added a *normalization layer* in front of the ResNet34 model, which performs a channel-wise transformation of an input by subtracting (0.485, 0.456, 0.406) (the mean of ImageNet) and then being divided by (0.229, 0.224, 0.225) (the standard deviation of ImageNet);² then, we train the neural networks as usual.

Unless otherwise specified, we used 60 epochs with training batch size 128 for Segment-6. For STL-10 and ImageNet-10, we trained the classifiers for 20 epochs by using a batch size of 64. We used Adam Optimizer (Kingma & Ba, 2014) with initial learning rate of 10^{-4} for *Clean*, and 10^{-3} for *AT-PGD* and *AT-Dual*, respectively. We dropped the learning rate by 0.1 every 20 epochs on Segment-6, and similarly at the 8th and 15th epochs on STL-10 and ImageNet-10.

¹Available at <https://pytorch.org/>.

²To fit the Segment-6 dataset which contains much smaller images compared to ImageNet, we also reset the first convolutional layer of the pre-trained ResNet34 model by reducing the kernel size from 7×7 to 3×3 , stride from 2 to 1, and pad from 3 to 1.

As mentioned above, we implemented *PGD* and *dual-perturbation* attacks, bounded by both ℓ_∞ and ℓ_2 norms, to evaluate robustness of a classification model, as well as to build robust classifiers. For ℓ_∞ attacks, when they were used for evaluation, they are performed with 20 steps; for training robust classifiers, these attacks were performed with 10 steps at each epoch of adversarial training. Similarly, for ℓ_2 attacks, they were performed with 100 steps for evaluation, and 50 steps for adversarial training. We used the semantic segmentation masks on the Segment-6 dataset and used fixation prediction to identify foreground and background on STL-10 and ImageNet-10.

D ADVERSARIAL TRAINING USING ℓ_2 NORM ATTACKS ON IMAGENET-10

Transferability of Adversarial Examples. Here, we measure the *transferability* of adversarial examples among different classification models. To do this, we first produced adversarial examples by using ℓ_2 PGD attack or dual-perturbation attack on a source model. Then, we used these examples to evaluate the performance of an independent target model, where a higher prediction accuracy means weaker transferability. The results are presented in Figure 7. The first observation is that dual-perturbation attacks exhibit significantly better transferability than the conventional PGD attacks (transferability is up to 40% better for dual-perturbation attacks). Second, we can observe that when *AT-Dual* is used as the target (i.e., defending by adversarial training with dual-perturbation examples), these are typically resistant to adversarial examples generated against either the clean model, or against *AT-PGD*. This observation obtains even when we use PGD to generate adversarial examples.

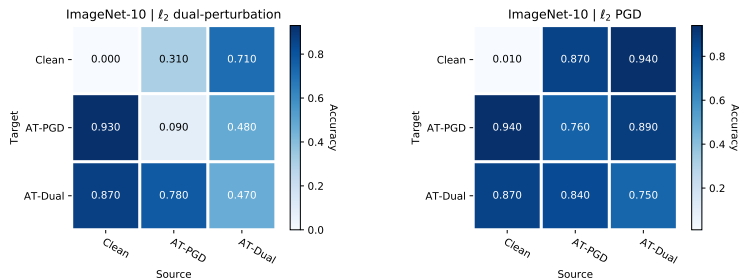


Figure 7: Robustness against adversarial examples transferred from other models on ImageNet-10. Left: ℓ_2 dual-perturbation attacks performed by using $\{\epsilon_F, \epsilon_B, \lambda\} = \{2.0, 20.0, 1.0\}$ on different source models. Right: ℓ_2 PGD attacks with $\epsilon = 2.0$ on different source models.

E ADVERSARIAL TRAINING USING ℓ_2 NORM ATTACKS ON STL-10

Here, we present experimental results of the robustness of classifiers that use adversarial training with ℓ_2 norm attacks on STL-10. Specifically, we trained AT-PGD using ℓ_2 PGD attack with $\epsilon = 1.0$, and AT-Dual by using ℓ_2 dual-perturbation attack with $\{\epsilon_F, \epsilon_B, \lambda\} = \{1.0, 5.0, 0.0\}$. The results are shown in Figure 8, 9, 10, and 11.

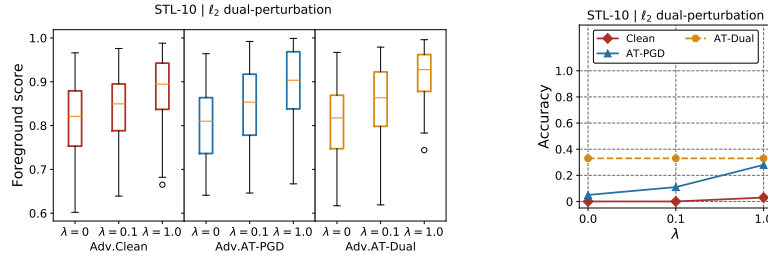


Figure 8: Saliency analysis. The ℓ_2 dual-perturbation attacks are performed by using $\{\epsilon_F, \epsilon_B\} = \{1.0, 5.0\}$, and a variety of λ displayed in the figure. Left: foreground scores of dual-perturbation examples in response to different classifiers. Right: accuracy of classifiers on dual-perturbation examples with saliency control.

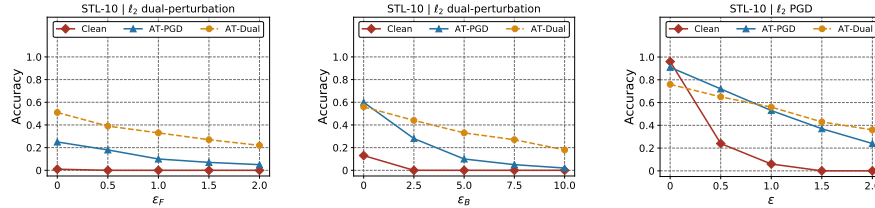


Figure 9: Robustness to white-box ℓ_2 attacks on STL-10. Left: ℓ_2 dual-perturbation attacks with different foreground distortions. ϵ_B is fixed to be 5.0 and $\lambda = 0.1$. Middle: ℓ_2 dual-perturbation attacks with different background distortions. ϵ_F is fixed to be 1.0 and $\lambda = 0.1$. Right: ℓ_2 PGD attacks.

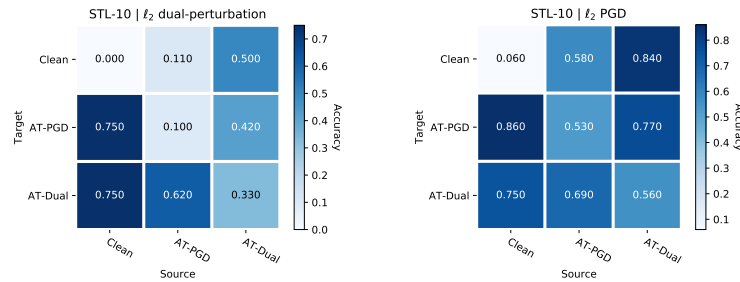


Figure 10: Robustness against adversarial examples transferred from other models on STL-10. Left: ℓ_2 dual-perturbation attacks performed by using $\{\epsilon_F, \epsilon_B, \lambda\} = \{1.0, 5.0, 0.1\}$ on different source models. Right: ℓ_2 PGD attacks with $\epsilon = 1.0$ on different source models.

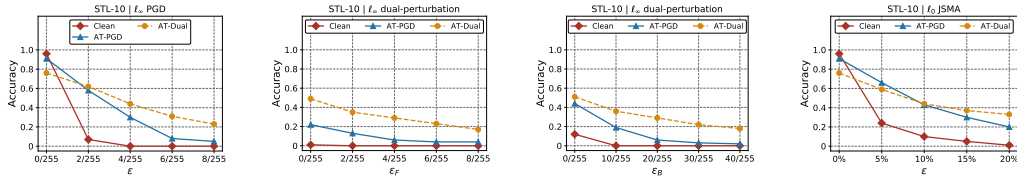


Figure 11: Robustness to additional white-box attacks on STL-10. Left: 20 steps of ℓ_∞ PGD attacks. Middle left: 20 steps of ℓ_∞ dual-perturbation attacks with different foreground distortions. ϵ_B is fixed to be $20/255$ and $\lambda = 0.1$. Middle right: 20 steps of ℓ_∞ dual-perturbation attacks with different background distortions. ϵ_F is fixed to be $4/255$ and $\lambda = 0.1$. Right: ℓ_0 JSMA attacks.

F ADVERSARIAL TRAINING USING ℓ_2 NORM ATTACKS ON SEGMENT-6

Now, we present experimental results of the robustness of classifiers that use adversarial training with ℓ_2 norm attacks on Segment-6. Since DeepGaze II only work on images with more than 35×35 pixels, we are unable to use DeepGaze II to compute the *foreground score* (FS) for Segment-6. Hence, in the following experiment on this dataset, we omit the saliency term in the optimization problem of Equation 3 and 4 in the main body of the paper. Specifically, we trained AT-PGD using ℓ_2 PGD attack with $\epsilon = 0.5$, and AT-Dual by using ℓ_2 dual-perturbation attack with $\{\epsilon_F, \epsilon_B\} = \{0.5, 2.5\}$. The results are shown in Figure 12, 13, and 14.

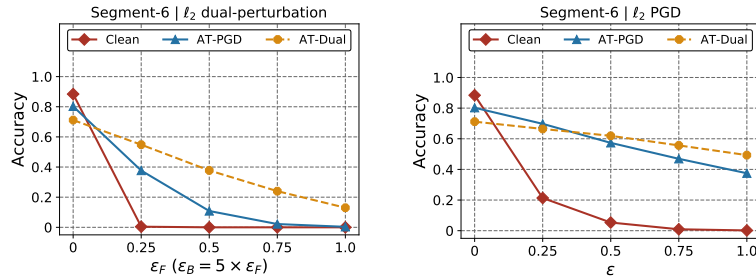


Figure 12: Robustness to white-box ℓ_2 attacks on Segment-6. Left: ℓ_2 dual-perturbation attacks with different foreground and background distortions. Right: ℓ_2 PGD attacks.

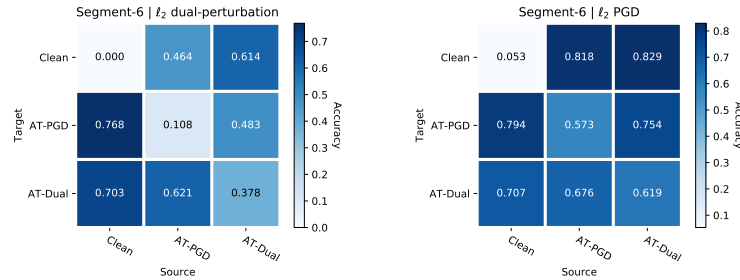


Figure 13: Robustness against adversarial examples transferred from other models on Segment-6. Left: ℓ_2 dual-perturbation attacks performed by using $\{\epsilon_F, \epsilon_B\} = \{0.5, 2.5\}$ on different source models. Right: ℓ_2 PGD attacks with $\epsilon = 0.5$ on different source models.

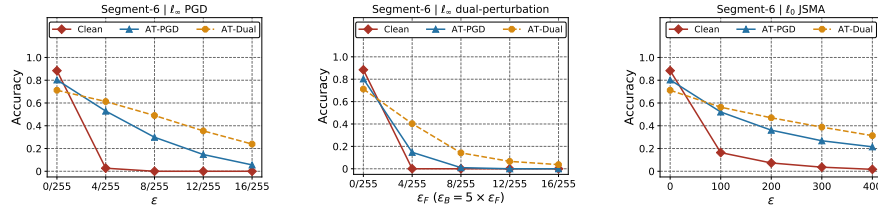


Figure 14: Robustness to additional white-box attacks on Segment-6. Left: 20 steps of ℓ_∞ PGD attacks. Middle: 20 steps of ℓ_∞ dual-perturbation attacks with different foreground and background distortions. Right: ℓ_0 JSMA attacks.

G ADVERSARIAL TRAINING USING ℓ_∞ NORM ATTACKS ON IMAGENET-10

Next, we present experimental results of the robustness of classifiers that use adversarial training with ℓ_∞ norm attacks on ImageNet-10. Specifically, we trained AT-PGD using ℓ_∞ PGD attack with $\epsilon = 4/255$, and AT-Dual by using ℓ_∞ dual-perturbation attack with $\{\epsilon_F, \epsilon_B, \lambda\} = \{4/255, 20/255, 0.0\}$. The results are shown in Figure 15, 16, 17, and 18.

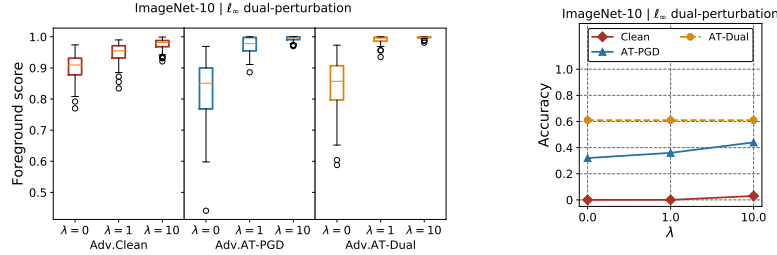


Figure 15: Saliency analysis. The ℓ_∞ dual-perturbation attacks are performed by using $\{\epsilon_F, \epsilon_B\} = \{4/255, 20/255\}$, and a variety of λ displayed in the figure. Left: foreground scores of dual-perturbation examples in response to different classifiers. Right: accuracy of classifiers on dual-perturbation examples with salience control.

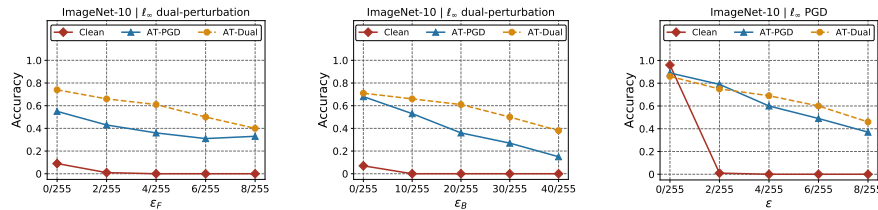


Figure 16: Robustness to white-box ℓ_∞ attacks on ImageNet-10. Left: ℓ_∞ dual-perturbation attacks with different foreground distortions. ϵ_B is fixed to be 20/255 and $\lambda = 1.0$. Middle: ℓ_∞ dual-perturbation attacks with different background distortions. ϵ_F is fixed to be 4/255 and $\lambda = 1.0$. Right: ℓ_∞ PGD attacks.

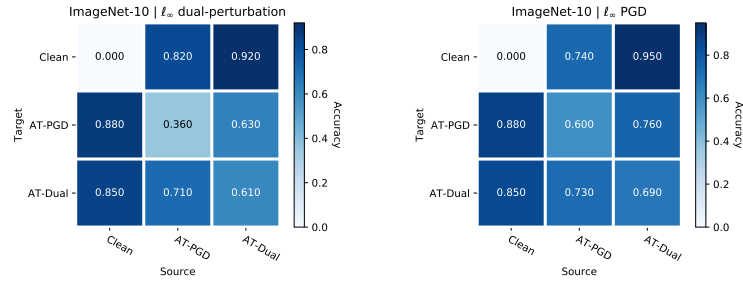


Figure 17: Robustness against adversarial examples transferred from other models on ImageNet-10. Left: l_∞ dual-perturbation attacks performed by using $\{\epsilon_F, \epsilon_B, \lambda\} = \{4/255, 20/255, 1.0\}$ on different source models. Right: l_∞ PGD attacks with $\epsilon = 4/255$ on different source models.

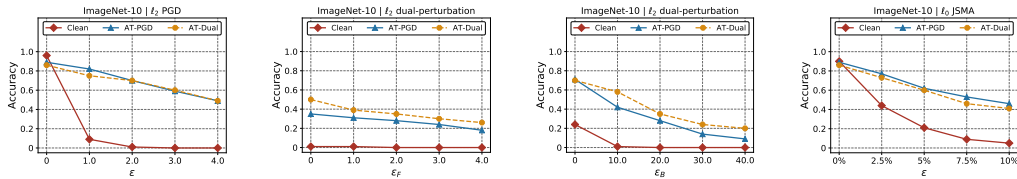


Figure 18: Robustness to additional white-box attacks on ImageNet-10. Left: 100 steps of l_2 PGD attacks. Middle left: 100 steps of l_2 dual-perturbation attacks with different foreground distortions. ϵ_B is fixed to be 2.0 and $\lambda = 1.0$. Middle right: 100 steps of l_2 dual-perturbation attacks with different background distortions. ϵ_F is fixed to be 20.0 and $\lambda = 1.0$. Right: l_0 JSMA attacks.

H ADVERSARIAL TRAINING USING l_∞ NORM ATTACKS ON STL-10

Now, we present experimental results of the robustness of classifiers that use adversarial training with l_∞ norm attacks on STL-10. Specifically, we trained AT-PGD using l_∞ PGD attack with $\epsilon = 4/255$, and AT-Dual by using l_∞ dual-perturbation attack with $\{\epsilon_F, \epsilon_B, \lambda\} = \{4/255, 20/255, 0.0\}$. The results are shown in Figure 19, 20, 21, and 22.

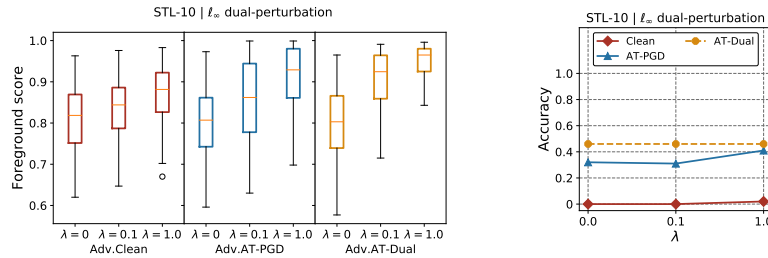


Figure 19: Saliency analysis. The l_∞ dual-perturbation attacks are performed by using $\{\epsilon_F, \epsilon_B\} = \{4/255, 20/255\}$, and a variety of λ displayed in the figure. Left: foreground scores of dual-perturbation examples in response to different classifiers. Right: accuracy of classifiers on dual-perturbation examples with salience control.

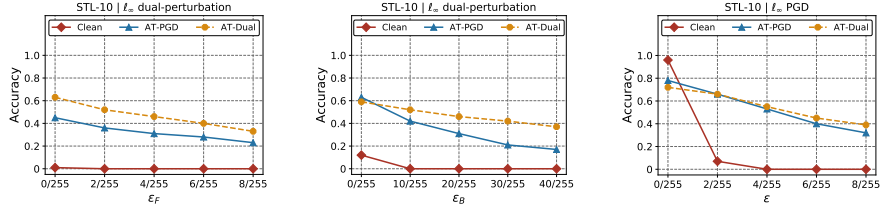


Figure 20: Robustness to white-box ℓ_∞ attacks on STL-10. Left: ℓ_∞ dual-perturbation attacks with different foreground distortions. ϵ_B is fixed to be 20/255 and $\lambda = 0.1$. Middle: ℓ_∞ dual-perturbation attacks with different background distortions. ϵ_F is fixed to be 4/255 and $\lambda = 0.1$. Right: ℓ_∞ PGD attacks.

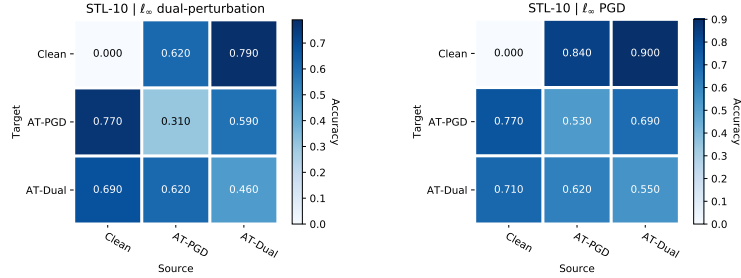


Figure 21: Robustness against adversarial examples transferred from other models on STL-10. Left: ℓ_∞ dual-perturbation attacks performed by using $\{\epsilon_F, \epsilon_B, \lambda\} = \{4/255, 20/255, 1.0\}$ on different source models. Right: ℓ_∞ PGD attacks with $\epsilon = 4/255$ on different source models.

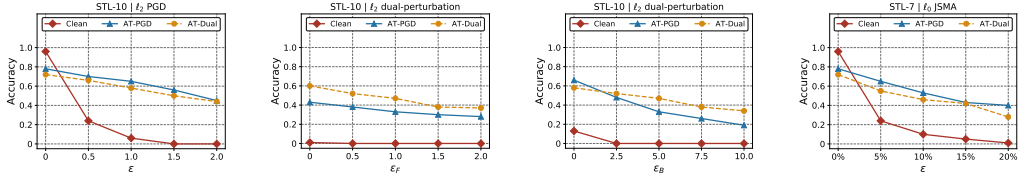


Figure 22: Robustness to additional white-box attacks on STL-10. Left: 100 steps of ℓ_2 PGD attacks. Middle left: 100 steps of ℓ_2 dual-perturbation attacks with different foreground distortions. ϵ_B is fixed to be 5.0 and $\lambda = 0.1$. Middle right: 100 steps of ℓ_2 dual-perturbation attacks with different background distortions. ϵ_F is fixed to be 1.0 and $\lambda = 0.1$. Right: ℓ_0 JSMA attacks.

I ADVERSARIAL TRAINING USING ℓ_∞ NORM ATTACKS ON SEGMENT-6

Finally, we present experimental results of the robustness of classifiers that use adversarial training with ℓ_∞ norm attacks on Segment-6. We trained AT-PGD using ℓ_∞ PGD attack with $\epsilon = 8/255$, and AT-Dual by using ℓ_∞ dual-perturbation attack with $\{\epsilon_F, \epsilon_B\} = \{8/255, 40/255\}$. The results are shown in Figure 23, 24, and 25.

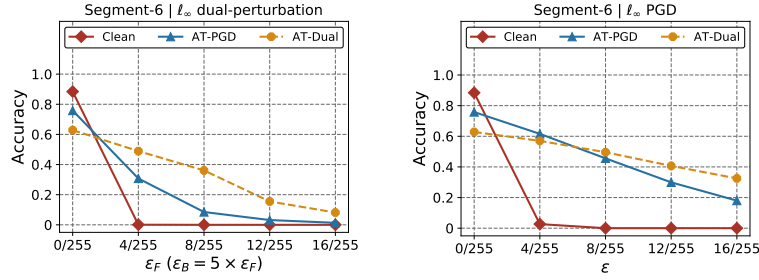


Figure 23: Robustness to white-box ℓ_∞ attacks on Segment-6. Left: ℓ_∞ dual-perturbation attacks with different foreground and background distortions. Right: ℓ_∞ PGD attacks.

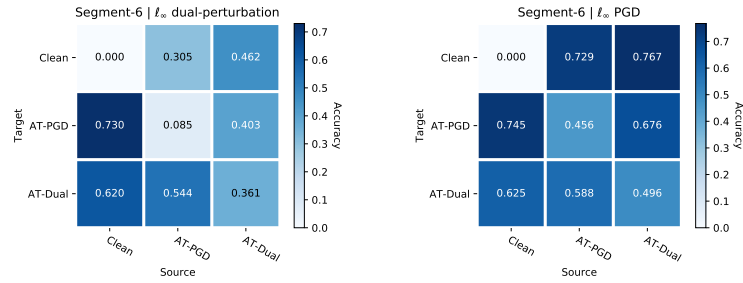


Figure 24: Robustness against adversarial examples transferred from other models on Segment-6. Left: ℓ_∞ dual-perturbation attacks performed by using $\{\epsilon_F, \epsilon_B\} = \{8/255, 40/255\}$ on different source models. Right: ℓ_∞ PGD attacks with $\epsilon = 8/255$ on different source models.

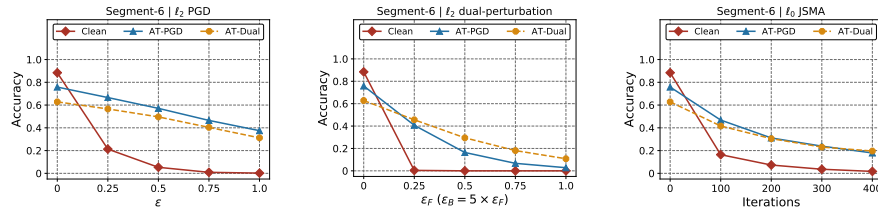


Figure 25: Robustness to additional white-box attacks on Segment-6. Left: 100 steps of ℓ_2 PGD attacks. Middle: 100 steps of ℓ_2 dual-perturbation attacks with different foreground and background distortions. Right: ℓ_0 JSMA attacks.

J ATTACKING RANDOMIZED CLASSIFIERS

In addition to *deterministic classifiers* that make a deterministic prediction for a test sample, our proposed attack can be adapted to *stochastic classifiers* that apply randomization at training and prediction time. For example, for classifiers using *randomized smoothing*, we can refine Equation 3 in the main body of the paper as follows:

$$\max_{\substack{\|\delta \circ \mathcal{F}(\mathbf{x})\|_p \leq \epsilon_F, \\ \|\delta \circ \mathcal{B}(\mathbf{x})\|_p \leq \epsilon_B}} \mathbb{E}_{\boldsymbol{\eta} \sim \mathcal{N}(\mathbf{0}, \sigma^2 \mathbf{I})} [\mathcal{L}(h_\theta(\mathbf{x} + \boldsymbol{\delta} + \boldsymbol{\eta}), y) + \lambda \cdot \mathcal{S}(\mathbf{x} + \boldsymbol{\delta} + \boldsymbol{\eta})], \quad (9)$$

where σ^2 is the variance of the Gaussian data augmentation in randomized smoothing.³ The optimization problem in Equation 9 can be solved by the same approach used for deterministic

³Note that the Gaussian perturbations are only used to compute the expectation of loss and are not in the resulting adversarial examples.

classifiers, with the following modification on Equation 7 at the second step in Section A:

$$\begin{cases} g_F = \mathcal{G}(\mathcal{F}(\mathbf{x}) \circ \nabla_{\delta^{(k)}} \mathbb{E}_{\boldsymbol{\eta}}[\mathcal{L}(h_{\theta}(\mathbf{x} + \delta^{(k)} + \boldsymbol{\eta}), y) + \lambda \cdot \mathcal{S}(\mathbf{x} + \delta^{(k)} + \boldsymbol{\eta})]) \\ g_B = \mathcal{G}(\mathcal{B}(\mathbf{x}) \circ \nabla_{\delta^{(k)}} \mathbb{E}_{\boldsymbol{\eta}}[\mathcal{L}(h_{\theta}(\mathbf{x} + \delta^{(k)} + \boldsymbol{\eta}), y) + \lambda \cdot \mathcal{S}(\mathbf{x} + \delta^{(k)} + \boldsymbol{\eta})]) \end{cases} \quad (10)$$

J.1 VARIANCE IN GAUSSIAN DATA AUGMENTATION

Table 4 and 5 show the effectiveness of *Randomized Smoothing (RS)* against the proposed dual-perturbation attack. Here, we use different variances in Gaussian data augmentation of *RS*, and fix the number of noise-corrupted copies at prediction time, n to be 100. It can be seen that *RS* is generally fragile to the dual-perturbation attacks that are adapted to randomized classifiers. Moreover, increasing σ , the variance used in Gaussian data augmentation can only marginally improve adversarial robustness to dual-perturbation attacks while significantly decrease accuracy on non-adversarial data.

Dataset	Defense approach	Attack Strength ($\epsilon_B = 5 \times \epsilon_F$)				
		$\epsilon_F = 0/255$	$\epsilon_F = 4/255$	$\epsilon_F = 8/255$	$\epsilon_F = 12/255$	$\epsilon_F = 1$
Segment-6	RS, $\sigma = 0.25$	71.4%	9.6%	0.4%	0.1%	0.0%
	RS, $\sigma = 0.5$	61.7%	13.7%	1.9%	0.6%	0.2%
	RS, $\sigma = 1$	47.7%	15.6%	2.8%	0.4%	0.2%

Table 4: Robustness of *RS* against ℓ_{∞} dual-perturbation attacks.

Defense approach	Attack Strength ($\epsilon_B = 5 \times \epsilon_F$)				
	$\epsilon_F = 0$	$\epsilon_F = 0.25$	$\epsilon_F = 0.5$	$\epsilon_F = 0.75$	$\epsilon_F = 1$
RS, $\sigma = 0.25$	71.4%	29.7%	6.7%	0.9%	0.1%
RS, $\sigma = 0.5$	61.7%	31.6%	11.8%	3.1%	1.3%
RS, $\sigma = 1$	47.7%	28.2%	14.4%	6.0%	1.5%

Table 5: Robustness of *RS* against ℓ_2 dual-perturbation attacks on Segment-6.

J.2 NUMBER OF SAMPLES WITH GAUSSIAN NOISE AT PREDICTION TIME

It has been observed that *Randomized Smoothing (RS)* can be computationally inefficient at prediction time as it uses a large number of noise-corrupted copies for each test sample at prediction time. It is natural to ask whether the prediction time of *RS* can be reduced without significantly sacrificing adversarial robustness in practice. We answer this question by studying the effectiveness of *RS* with different n , the numbers of noise-corrupted copies at prediction time. Specifically, we fix $\sigma = 0.5$ and set n to be 1, 25, and 100. Note that when $n = 1$, there is no two-sided hypothesis test for prediction; thus, no abstentions are obtained.

Here we use ℓ_{∞} dual-perturbation attacks on *RS* for demonstration purposes. The results are shown in Table 6. It can be seen that when $n = 25$, the accuracy on both adversarial and non-adversarial data can drop by up to 10% compared to *RS* using $n = 100$. The reason is that under a small n , the prediction appears more likely to abstain. Interestingly, when $n = 1$, the accuracy can be marginally improved compared to $n = 100$, with the prediction time being reduced by 99%. This indicates that in practice, we would not lose accuracy without using the two-sided hypothesis test at prediction time.

Dataset	Defense approach	Attack Strength ($\epsilon_B = 5 \times \epsilon_F$)				
		$\epsilon_F = 0/255$	$\epsilon_F = 4/255$	$\epsilon_F = 8/255$	$\epsilon_F = 12/255$	$\epsilon_F = 1$
Segment-6	RS, $n = 1$	66.0%	19.8%	3.2%	0.8%	0.3%
	RS, $n = 25$	49.4%	9.1%	1.3%	0.5%	0.0%
	RS, $n = 100$	61.7%	13.7%	1.9%	0.6%	0.2%

Table 6: Robustness of *RS* against ℓ_{∞} dual-perturbation attacks under different numbers of noise-corrupted copies at prediction time.

K VISUALIZATION OF LOSS GRADIENT

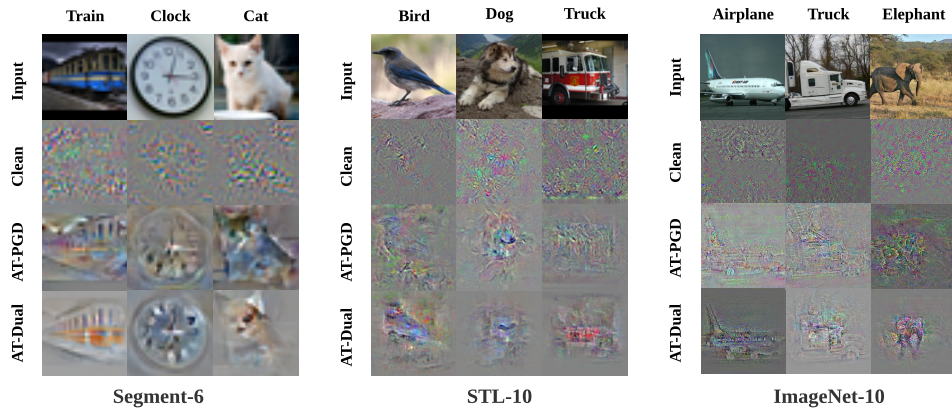


Figure 26: Visualization of loss gradient of different classifiers with respect to pixels of *non-adversarial* inputs. AT-PGD and AT-Dual were obtained using adversarial training with corresponding ℓ_2 norm attacks.

L EXAMPLES OF DUAL-PERTURBATION ATTACKS

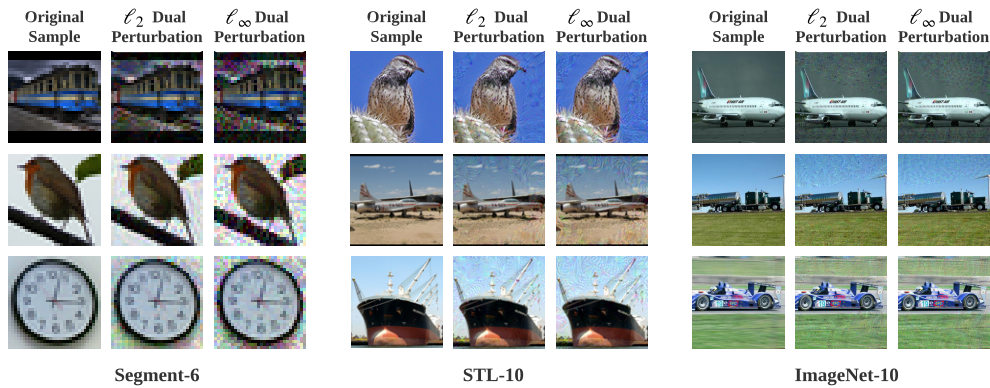


Figure 27: Dual-perturbation attacks. Adversarial examples are produced in response to the *Clean* model for each dataset.